Letter

Extended quantum process tomography of logical operations on an encoded bosonic qubit

Mikael Kervinen, Shahnawaz Ahmed, Marina Kudra, Axel Eriksson, Fernando Quijandría,* Anton Frisk Kockum, Per Delsing,† and Simone Gasparinetti‡

Department of Microtechnology and Nanoscience, Chalmers University of Technology, 412 96 Gothenburg, Sweden

(Received 9 April 2024; accepted 14 June 2024; published 14 August 2024)

We demonstrate the use of coherent-state quantum process tomography (csQPT) for a bosonic-mode superconducting circuit. We have enhanced our methodology over previous implementations of csQPT by leveraging Kraus operators and constrained gradient descent to learn the underlying process. We show the results of our method by characterizing a logical quantum gate implemented using displacement and selective number-dependent arbitrary phase operations on an encoded qubit. Our use of csQPT allows for the reconstruction of Kraus operators for the larger Hilbert space rather than being limited to the logical subspace. This approach enables us to more accurately identify and quantify the various error mechanisms that can lead to gate infidelity, including those occurring outside of the computational subspace. We showcase the potential of our approach by demonstrating the ability to quantify leakage outside of the computational subspace, a key factor for developing more robust and reliable quantum gates in high-dimensional systems.

DOI: 10.1103/PhysRevA.110.L020401

As quantum computing architectures become more refined, there is a surge of demand for methods to accurately characterize quantum gates and the processes limiting their performance. To meet this demand, methods like quantum process tomography [1], randomized benchmarking [2], and gate-set tomography [3] have been developed and tested on single-qubit [4], two-qubit [5], and three-qubit gates [6]. At the same time, an alternative approach to quantum computing relies on encoding quantum information in harmonic oscillators, also referred to as continuous-variable systems, or bosonic modes [7]. In contrast to two-level systems, the large Hilbert space of harmonic oscillators leaves a freedom in the choice of states in which to encode the information. This freedom can be exploited to render the encoded information robust against photon loss, the dominant source of error in oscillators, opening the door to hardware-efficient quantum error correction [8] and error-transparent or fault-tolerant gates [9–11].

Compared to the two-level paradigm, the development of high-fidelity quantum gates and their characterization in bosonic modes is still at an early stage [12,13]. In state-of-the-art experiments with superconducting circuits, quantum gates in bosonic modes are characterized by sandwiching the gate under test by encoding and decoding operations [14]. These operations establish a mapping between the logical states of the qubit encoded in the oscillator and the states of an ancillary qubit, which can be more easily manipulated and read out. However, this technique suffers from serious limitations. First, the encoding and decoding operations are complex entangling gates whose fidelities are not guaranteed to exceed that of the gate under test, leading to significant state preparation and measurement (SPAM) errors. In addition, the decoding operation, followed by readout of the ancillary qubit, reduces the full Hilbert space of the oscillator to that of a two-level system. This reduction hinders the possibility to reliably distinguish between different types of errors, as well as to characterize leakage errors [15].

Here, we experimentally demonstrate the use of coherent-state quantum process tomography (csQPT) to characterize a quantum gate in a continuous-variable system. The gate acts on a logical qubit encoded in a bosonic mode, which is hosted by a microwave cavity in a superconducting circuit architecture. Typically in harmonic oscillators, coherent states are the simplest states to prepare. By letting the gate under test act on a set of coherent-state probes and measuring the final states by direct Wigner tomography, we completely characterize the process in the Fock space of the oscillator.

CsQPT was proposed and first implemented for quantum optical processes using homodyne tomography followed by maximum likelihood reconstruction [16,17]. To decrease the measurement overhead, we improve on maximum-likelihood csQPT [18] by augmenting csQPT with a gradient-descent based learning algorithm using the idea of manifold learning [19]. This method allows us to reconstruct quantum process matrices from a reduced number of data points, avoiding full state tomography. From the process matrices, we can generate any representation of the process, determine the

*Present address: Quantum Machines Unit, Okinawa Institute of Science and Technology Graduate University, Onna-son, Okinawa 904-0495, Japan.

†Contact author: per.delsing@chalmers.se

‡Contact author: simoneg@chalmers.se

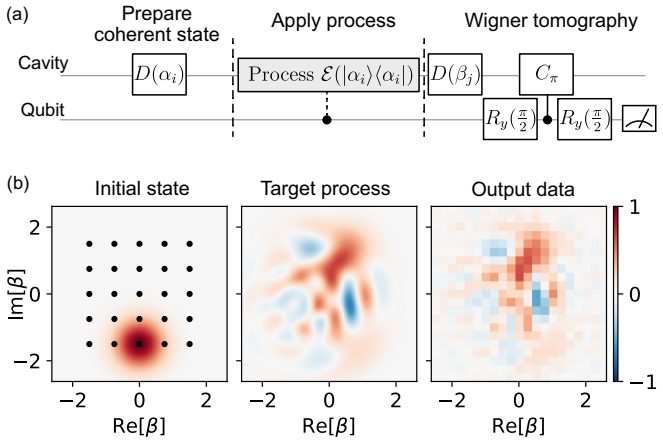

FIG. 1. Protocol for the csQPT. (a) Gate sequence for the process-tomography protocol. The probe states are coherent states in a 5×5 grid of complex displacements α_i [see the left plot in panel (b)]. The process $\mathcal{E}$ is applied to each probe state. Finally, the cavity state is measured using Wigner tomography. The Wigner tomography consists of a cavity displacement D(β_j), unconditional qubit $\frac{\pi}{2}$ pulse, conditional phase evolution C_π, and another qubit $\frac{\pi}{2}$ pulse followed by a readout. (b) Wigner functions at each step of the protocol. The middle panel shows the ideal target result of applying the process $\mathcal{E}$ to the coherent-state probe visualized in the left panel. The right panel shows data points denoting the values of the Wigner function in a 21×21 grid of complex displacements β_j. The Wigner-function measurements are repeated for each input probe.

process fidelity of the gate, and characterize the leakage outside of the computational subspace. Our approach goes beyond encoding-decoding schemes in two ways: it reduces SPAM errors by obviating the need for complex encoding and decoding operations, and it unlocks the access to the larger Hilbert space of the continuous-variable system, making it possible to correctly identify leakage errors.

Continuous-variable systems realized in particular with superconducting three-dimensional (3D) cavities coupled to an ancilla qubit have shown an unprecedented level of versatile control of quantum states [14,20–23]. We implement csQPT on a system consisting of a single-mode 3D superconducting $\lambda/4$ cavity [24,25] and an ancilla transmon qubit [26]. The transmon qubit is used to provide a nonlinear control element which is necessary in order to control the harmonic energy levels of the cavity, as well as provide means to characterize the cavity states through direct Wigner tomography [20]. The transmon qubit with its own readout resonator is fabricated on a sapphire chip, and the chip is inserted into the cavity, where the qubit and the cavity are capacitively coupled.

To perform csQPT, we run experimental sequences consisting of three steps [Fig. 1(a)]. First, we prepare the cavity in a coherent state $|\alpha_i\rangle$—our input probe. We create coherent states by passive thermalization to the ground (vacuum) state $|0\rangle$ followed by a displacement operation $D(\alpha_i)$. Next, we apply the quantum process $\mathcal{E}$ that we intend to characterize to the input state. Finally, we measure a displaced parity operator with the assistance of the ancillary qubit. To do so, we apply a displacement $D(\beta_j)$ to the cavity and then measure its photon parity by performing a Ramsey measurement that maps the parity to the σ_z axis of the qubit [20]. Averaging over this sequence and varying β_j to map different regions of the phase space gives a direct measurement of the Wigner function $W(\beta)$ of the coherent state $|\alpha_i\rangle$, after it has been acted upon by the gate. We repeat this procedure for a rectangular 5×5 grid array of coherent-state probes spanning from $-1.5 - 1.5i$ to $1.5 + 1.5i$ [Fig. 1(b)]. The amplitude of the coherent-state probes determines the maximum photon number that is populated and thereby sets a limit on the size of the cavity Hilbert space in which we can reliably reconstruct the process. We find our choice of the probe amplitude to be sufficient to reconstruct the process up to Fock state $|5\rangle$ (see Supplemental Material [27]).

The reconstruction of a process representation for $\mathcal{E}$ is performed using a gradient-based optimization that learns the Kraus representation of the process [19]. The Kraus operators are learned by minimizing a loss function that is the squared error between the measured Wigner data points and the corresponding Wigner points predicted by the reconstructed Kraus operators. Our optimization procedure is constrained to the manifold of completely positive and trace-preserving quantum operations with appropriate restrictions on the Kraus operators [27]. Reconstructing the process at the Kraus level allows us to limit the size of the process representation by restricting the number of Kraus operators. We therefore limit our reconstruction to a low rank, so that we can learn the dominant process channels without having to reconstruct the full-rank process. Additionally, the noise in the data may not allow the reconstruction of all the loss channels even if more Kraus operators are introduced. With this method, we can reconstruct the Kraus operators directly without an intermediate step of reconstructing the density matrices of the output states.

We test csQPT on a quantum logical gate that swaps the population of the states $|0_L\rangle$ and $|1_L\rangle$, i.e., a logical X gate (Fig. 2). We choose the binomial encoding

$$|0_L\rangle = |2\rangle,$$
$$|1_L\rangle = \frac{1}{\sqrt{2}}(|0\rangle + |4\rangle),$$

which is the lowest-order binomial code that can be corrected for the single-photon loss error in the cavity [28]. We implement the gate as a series of displacement $D(\alpha)$ and selective number-dependent arbitrary phase (SNAP) operations $S(\theta)$ [29]. These two operations provide universal control of the cavity states [30]. We numerically optimize the gate sequence [31] and the pulse envelopes following the method described in Ref. [23], which was shown to reduce the gate length while making the pulses more robust against variations of the system parameters. In SNAP gates, the qubit starts and ends in the ground state with high probability regardless of the initial state of the cavity, so that the same qubit becomes available for the Wigner-tomography measurement protocol. Previously, SNAP and displacement operations had only been used in the context of state preparation. Here, we show that these operations can also be used to efficiently implement logical gates. In particular, we implement the X gate with only three SNAP gates and four displacements. Compared to gate implementations based on fully numerical optimal

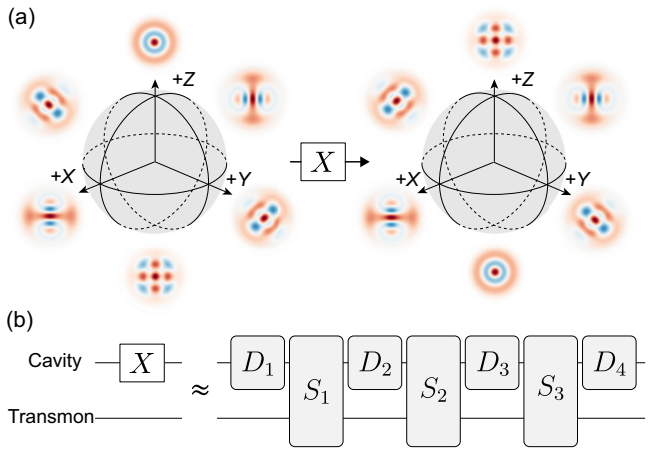

FIG. 2. X gate in binomial encoding. (a) The gate is defined by mapping the six cardinal states in the encoded subspace to their respective targets. The gate is defined only for the encoded subspace, but we can characterize it generally by analyzing its action on the large Hilbert space and not just the cardinal states. (b) The X gate for the cavity-encoded logical state is composed of three SNAP operations and four displacement operations.

control, in which the transmon-cavity composite system is driven simultaneously [14,28], separate gates on the cavity and on the transmon are more easily parametrized, the effects of the individual operations are more transparent [23], and they can be made more easily tolerant against transmon decoherence [10,11].

We characterize the X gate by running the process tomography sequence and process reconstruction described above. From the obtained Kraus operators, we construct the population transfer matrix (Fig. 3). The elements of the matrix

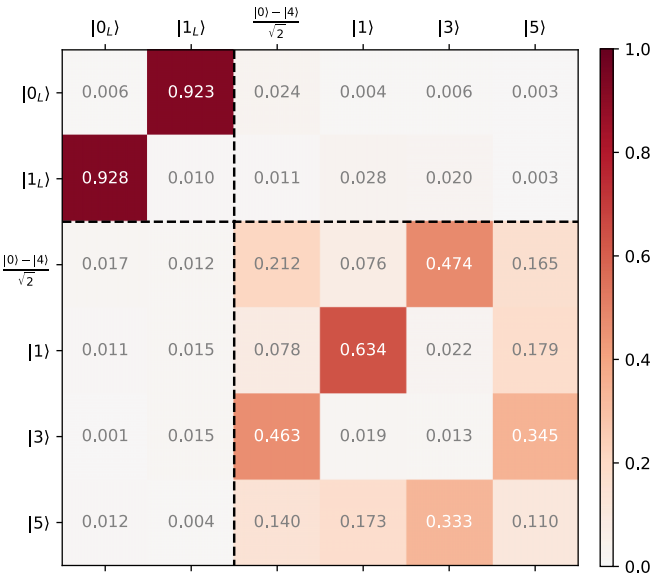

FIG. 3. Population transfer matrix. The upper-left block represents the logical subspace, where we can identify the X gate that swaps states $|0_L\rangle$ and $|1_L\rangle$. The columns correspond to the input states, while rows correspond to the output states.

describe the population distribution of the final state in a chosen basis, given one of the basis states was prepared as the initial state. Instead of the usual Fock basis, the matrix is presented in a basis given by $\{|0_L\rangle, |1_L\rangle, \frac{1}{\sqrt{2}}(|0\rangle - |4\rangle), |1\rangle, |3\rangle, |5\rangle\}$, which transparently shows the effect on the logical basis vectors. We have truncated the matrix representation to five excitations, since our gate under test is photon number preserving with a maximum occupied Fock state of $|4\rangle$, and with our choice of probes we can reliably characterize the process up to Fock state $|5\rangle$ [27]. In this representation, we identify the X gate in the logical subspace in the upper-left block of the population matrix. By inspecting the matrix entries we can quantify the amount of population transfer within the logical subspace. We see that the swap operation between $|0_L\rangle$ and $|1_L\rangle$ is successful, with a population transfer between 92 and 93 % and a population loss on the order of 7 % . The elements underneath the logical states describe population leakage outside of the computational subspace. For example, when preparing $|0_L\rangle$, we observe that most of the population loss is due to leakage to states outside of the computational subspace. The largest leakage is into $\frac{1}{\sqrt{2}}(|0\rangle - |4\rangle)$, which is one of the no-jump evolution error states of the binomial code [32]. Similarly, the largest leakage from $|1_L\rangle$ is into $|1\rangle$ and $|3\rangle$, which are the main error states of the binomial code.

The population transfer matrix does not describe the coherence between the chosen basis states. As such, it only offers a partial representation of the quantum process. To provide a complete description of the process $\mathcal{E}$, we use a generalization of the Pauli transfer matrix from two-level systems to d-level systems. We refer to this generalization as the Gell-Mann transfer matrix [27]. We show the transfer matrix in Fig. 4, where we have only included the elements that couple to the logical states up to a Fock state $|5\rangle$. In the upper-left corner of the Gell-Mann transfer matrix, we can identify a Pauli-transfer-matrix-like block of an X gate for the two-level logical subsystem. In Fig. 4(b), we present the experimental Pauli transfer matrix that is calculated from the Kraus operators alongside the simulated and ideal transfer matrices. Coherent errors within the logical subspace appear as off-diagonal elements in the Pauli transfer matrix for this particular gate. The detailed information of the leakage out of (into) the logical subspace is given by the off-diagonal blocks below (next to) the computational subspace [33].

We can now calculate the average gate fidelity [34] between the reconstructed process $\mathcal{E}$ and the targeted logical gate U in the $(d = 2)$-dimensional logical subspace, also considering leakage, as

$$F_g(\mathcal{E}, U) = \frac{dF_{\text{pro}}(\mathcal{E}, U) + 1 - L_L(\mathcal{E})}{d + 1}. \tag{1}$$

Here $F_{\text{pro}}(\mathcal{E}, U)$ is the process fidelity, which can be written down using any representation of the process $\mathcal{E}$, e.g., the Kraus operators [1], the Choi matrix [35], or the Pauli transfer matrix [36]. The average leakage rate is defined as $L_L(\mathcal{E}) = \int d\psi_L \mathcal{E}(|\psi_L\rangle\langle\psi_L|) = L[\mathcal{E}(\frac{\mathbb{I}_L}{d})]$ [37], where $L(\rho) = 1 - \text{Tr}[\mathbb{I}_L\rho]$ quantifies the leakage from the logical subspace and the integral is over all states in the logical subspace. The unitary $U = |0_L\rangle\langle 1_L| + |1_L\rangle\langle 0_L|$ represents the logical X gate and the projector $\mathbb{I}_L = |0_L\rangle\langle 0_L| + |1_L\rangle\langle 1_L|$ is the identity in

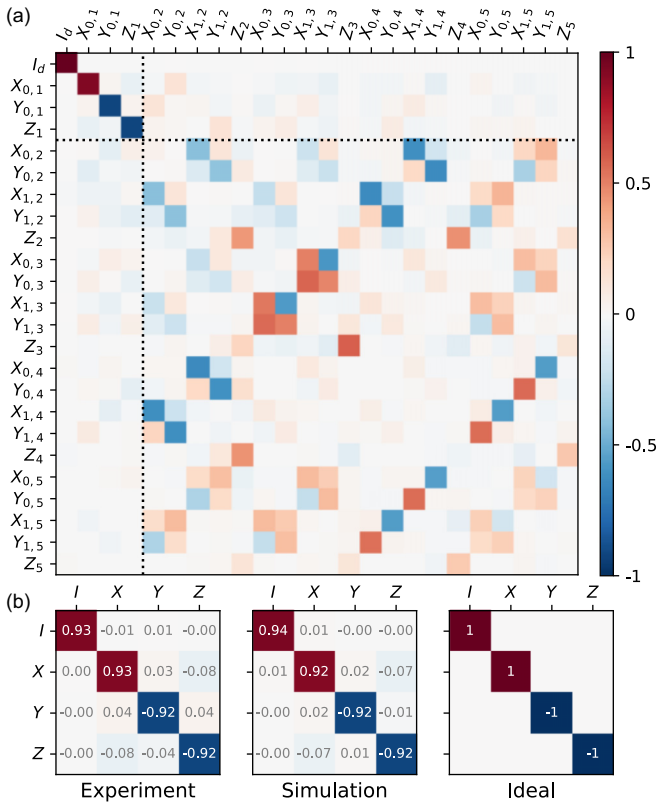

FIG. 4. Gell-Mann transfer matrix of an X gate. (a) The upper-left block represents a Pauli-transfer-matrix-like structure for the logical subspace. The other elements in the Gell-Mann transfer matrix represent couplings between different levels of the system. They are given in a basis defined by the Gell-Mann matrices. (b) Comparison of the experimental (reconstructed), simulated, and ideal two-level Pauli transfer matrices that are obtained by restricting the Gell-Mann transfer matrix to the logical subspace.

the logical subspace. We can write Eq. (1) using the Kraus representation of the process in the full Hilbert space (see Appendixes), providing us information about the leakage out from the computational subspace. The average population leakage out of the computational subspace is calculated to be 6.6 % . The average gate fidelity obtained from the reconstructed process is $F_g(\mathcal{E}, U) = 92.8\,\%$. In order to estimate the effects of decoherence with known parameters of our system, we calculate the average gate fidelity from Lindblad master-equation simulations, with our measured decoherence rates. We obtain an expected gate fidelity of 92.9 % from the simulations, which is in close agreement with the average gate fidelity given by our method. We thus show an experimental demonstration that relatively high-fidelity logical quantum gates can be composed of displacement and SNAP operations.

With continuous-variable gates, the leakage into energy levels outside of the computational basis presents a problem that needs to be carefully addressed. With our method, we avoid a large component in the error estimation that comes from estimating the dimension of the Hilbert space that the errors leak into [14]. We foresee that with further analysis of the Gell-Mann transfer matrix, more detailed error analysis can be performed. In particular, having access to the process-matrix elements beyond the logical subspace opens up possibilities to study different error models in order to more accurately pinpoint the origin of the gate infidelity [33]. Our results establish the use of csQPT to understand the error mechanisms affecting continuous-variable quantum gates, paving the way towards better-performing bosonic codes. Our method can also be directly applied to simultaneously characterize the effect of a certain operation on both the code subspace and the error subspace, which could assist the design of quantum error correction sequences.

Acknowledgments. We would like to thank M. Myremark and L. Jönsson for machining the cavity, and A. Osman for fabricating a similar qubit chip. The simulations and visualization of the quantum states were performed using QUTIP [38,39], NUMPY [40], and MATPLOTLIB [41]. The automatic differentiation tool JAX [42] was used for process reconstruction and the optimization of gate parameters. This work was supported by the Knut and Alice Wallenberg foundation via the Wallenberg Centre for Quantum Technology and by the Swedish Research Council. The chips were fabricated at the Chalmers Myfab cleanroom. We acknowledge Intelligence Advanced Research Projects Activity (IARPA) and Lincoln Labs for providing the traveling wave parametric amplifier (TWPA) used in this experiment.

Appendix A: Kraus representation of a quantum process. In general, a quantum process is described by a completely positive trace-preserving map $\mathcal{E}$ between the input and output states. This map can be represented with Kraus operators K_i as

$$\rho' = \mathcal{E}(\rho) = \sum_i^r K_i \rho K_i^\dagger. \tag{A1}$$

The number r of Kraus operators can take values from 1, which corresponds to a unitary process, up to d^2 in a Hilbert space with dimension d. The Kraus representation ensures the complete positivity of the process. Trace preservation is imposed by satisfying the constraint

$$\sum_i^r K_i^\dagger K_i = \mathbb{I}. \tag{A2}$$

Appendix B: Gell-Mann transfer matrix. Similar to the ($d = 2$) Pauli transfer matrix [36], we define the Gell-Mann transfer matrix of a process $\mathcal{E}$ as a single real-valued matrix $\Lambda^{\mathcal{E}}$, whose elements are bounded between -1 and $+1$. The Gell-Mann matrices $\{G_i\}$ [43], including the identity matrix, form an operator basis for the symmetry group $SU(d)$ similar to how the Pauli matrices generate arbitrary unitaries in $SU(2)$. The Gell-Mann transfer matrix is computed by applying the quantum process to the Gell-Mann matrices and then computing the matrix elements $\Lambda_{ij}^{\mathcal{E}}$ as

$$\Lambda_{ij}^{\mathcal{E}} = \frac{1}{d}\mathrm{Tr}[G_j \mathcal{E}(G_i)]. \tag{B1}$$

We can then write the action of the process on some quantum state ρ using the Gell-Mann transfer matrix, by vectorizing ρ using the operator basis consisting of the Gell-Mann matrices, as $\mathcal{E}(\rho) = \Lambda^{\mathcal{E}}\vec{\rho}$ with the elements of the vectorized density matrix given by $(\vec{\rho})_i = \mathrm{Tr}[G_i\rho]$.

Appendix C: Average gate fidelity for the logical subspace. The average gate fidelity between a unitary operation U

representing a quantum gate and a process $\mathcal{E}$ can be defined as [34]

$$F_g(\mathcal{E}, U) = \int d|\psi\rangle\langle\psi|U^\dagger \mathcal{E}(|\psi\rangle\langle\psi|)U|\psi\rangle, \tag{C1}$$

where the integral is over the set of all input states $|\psi\rangle = \sum_n c_n|n\rangle$ with $c_n \in \mathbb{C}$ and $\sum_n |c_n|^2 = 1$. Using the Kraus representation for the process $\mathcal{E}$ we can generally write the integral as

$$\begin{aligned} F_g(\mathcal{E}, U) &= \sum_i \int d|\psi\rangle\langle\psi|U^\dagger K_i|\psi\rangle\langle\psi|K_i^\dagger U|\psi\rangle \\ &= \sum_i \sum_{klmn} \langle k|U^\dagger K_i|l\rangle\langle m|K_i^\dagger U|n\rangle \int d|\psi\rangle c_k^* c_l c_m^* c_n \\ &= \sum_i \sum_{klmn} \langle k|U^\dagger K_i|l\rangle\langle m|K_i^\dagger U|n\rangle \frac{(\delta_{kl}\delta_{mn} + \delta_{kn}\delta_{lm})}{d(d+1)} \end{aligned} \tag{C2}$$

where the value of the integral $\int d|\psi\rangle c_k^* c_l c_m^* c_n = \frac{(\delta_{kl}\delta_{mn}+\delta_{kn}\delta_{lm})}{d(d+1)}$ over the set of input states. This integral can be evaluated in several ways [44]; one of the simplest is to reduce it to a set of Gaussian integrals [45]. In order to obtain a simple analytical expression for $F_g(\mathcal{E}, U)$, we can identify the various terms as taking the trace in the logical subspace such that

$$\begin{aligned} F_g(\mathcal{E}, U) &= \sum_i \sum_{km} \langle k|U^\dagger K_i|k\rangle\langle m|K_i^\dagger U|m\rangle \frac{1}{d(d+1)} \\ &\quad + \sum_i \sum_{kl} \langle k|U^\dagger K_i|l\rangle\langle l|K_i^\dagger U|k\rangle \frac{1}{d(d+1)} \\ &= \sum_i \frac{|\mathrm{Tr}[U^\dagger K_i]|^2 + \mathrm{Tr}[U^\dagger K_i(\sum_l |l\rangle\langle l|)K_i^\dagger U]}{d(d+1)} \\ &= \frac{\sum_i |\mathrm{Tr}[U^\dagger K_i]|^2 + \mathrm{Tr}[U^\dagger \mathcal{E}(\mathbb{I}_L)U]}{d(d+1)} \\ &= \frac{\sum_i |\mathrm{Tr}[U^\dagger K_i]|^2 + d\mathrm{Tr}\left[\mathbb{I}_L \mathcal{E}\left(\frac{\mathbb{I}_L}{d}\right)\right]}{d(d+1)}. \end{aligned} \tag{C3}$$

Since we are interested in the average gate fidelity within the logical subspace, we only consider states in the logical basis as $|\psi\rangle = |\psi_L\rangle = c_0|0_L\rangle + c_1|1_L\rangle$ such that the identity operation is given by $\mathbb{I}_L = \sum_l |l\rangle\langle l| = |0_L\rangle\langle 0_L| + |1_L\rangle\langle 1_L|$. We have used the property that taking the trace is invariant to a basis transformation such that we can write U and K_i in any basis. We have also used the cyclic property of the trace to write $\mathrm{Tr}[U^\dagger \mathcal{E}(\mathbb{I}_L)U] = \mathrm{Tr}[U^\dagger U \mathcal{E}(\mathbb{I}_L)] = d\mathrm{Tr}[\mathbb{I}_L \mathcal{E}(\frac{\mathbb{I}_L}{d})]$ in the last step.

We can easily reduce Eq. (C3) to Eq. (1) from Ref. [37] by identifying the process fidelity in terms of Kraus operators as [1]

$$F_{\mathrm{pro}}(\mathcal{E}, U) = \frac{\sum_i |\mathrm{Tr}[U^\dagger K_i]|^2}{d^2}, \tag{C4}$$

such that Eq. (C3) can be written as

$$\begin{aligned} F_g(\mathcal{E}, U) &= \frac{d^2 F_{\mathrm{pro}}(\mathcal{E}, U) + d\mathrm{Tr}\left[\mathbb{I}_L \mathcal{E}\left(\frac{\mathbb{I}_L}{d}\right)\right]}{d(d+1)} \\ &= \frac{dF_{\mathrm{pro}}(\mathcal{E}, U) + 1 - L_L(\mathcal{E})}{d+1}. \end{aligned} \tag{C5}$$

[1] M. A. Nielsen and I. L. Chuang, *Quantum Computation and Quantum Information: 10th Anniversary Edition* (Cambridge University, New York, 2010).

[2] E. Magesan, J. M. Gambetta, and J. Emerson, Scalable and robust randomized benchmarking of quantum processes, Phys. Rev. Lett. **106**, 180504 (2011).

[3] D. Greenbaum, Introduction to quantum gate set tomography, arXiv:1509.02921.

[4] J. M. Chow, J. M. Gambetta, L. Tornberg, J. Koch, L. S. Bishop, A. A. Houck, B. R. Johnson, L. Frunzio, S. M. Girvin, and R. J. Schoelkopf, Randomized benchmarking and process tomography for gate errors in a solid-state qubit, Phys. Rev. Lett. **102**, 090502 (2009).

[5] D. C. McKay, S. Filipp, A. Mezzacapo, E. Magesan, J. M. Chow, and J. M. Gambetta, Universal gate for fixed-frequency qubits via a tunable bus, Phys. Rev. Appl. **6**, 064007 (2016).

[6] C. W. Warren, J. Fernández-Pendás, S. Ahmed, T. Abad, A. Bengtsson, J. Biznárová, K. Debnath, X. Gu, C. Križan, A. Osman *et al.*, Extensive characterization of a family of efficient three-qubit gates at the coherence limit, npj Quantum Inf. **9**, 44 (2023).

[7] A. Joshi, K. Noh, and Y. Y. Gao, Quantum information processing with bosonic qubits in circuit QED, Quantum Sci. Technol. **6**, 033001 (2021).

[8] B. M. Terhal, J. Conrad, and C. Vuillot, Towards scalable bosonic quantum error correction, Quantum Sci. Technol. **5**, 043001 (2020).

[9] S. Rosenblum, P. Reinhold, M. Mirrahimi, L. Jiang, L. Frunzio, and R. J. Schoelkopf, Fault-tolerant detection of a quantum error, Science **361**, 266 (2018).

[10] P. Reinhold, S. Rosenblum, W.-L. Ma, L. Frunzio, L. Jiang, and R. J. Schoelkopf, Error-corrected gates on an encoded qubit, Nat. Phys. **16**, 822 (2020).

[11] Y. Ma, Y. Xu, X. Mu, W. Cai, L. Hu, W. Wang, X. Pan, H. Wang, Y. Song, C.-L. Zou *et al.*, Error-transparent operations on a logical qubit protected by quantum error correction, Nat. Phys. **16**, 827 (2020).

[12] W. Cai, Y. Ma, W. Wang, C.-L. Zou, and L. Sun, Bosonic quantum error correction codes in superconducting quantum circuits, Fundam. Res. **1**, 50 (2021).

[13] W.-L. Ma, S. Puri, R. J. Schoelkopf, M. H. Devoret, S. Girvin, and L. Jiang, Quantum control of bosonic modes with superconducting circuits, Sci. Bull. **66**, 1789 (2021).

[14] R. W. Heeres, P. Reinhold, N. Ofek, L. Frunzio, L. Jiang, M. H. Devoret, and R. J. Schoelkopf, Implementing a universal gate set on a logical qubit encoded in an oscillator, Nat. Commun. **8**, 94 (2017).

[15] J. J. Wallman, M. Barnhill, and J. Emerson, Robust characterization of leakage errors, New J. Phys. **18**, 043021 (2016).

[16] M. Lobino, D. Korystov, C. Kupchak, E. Figueroa, B. C. Sanders, and A. Lvovsky, Complete characterization of quantum-optical processes, Science **322**, 563 (2008).
[17] S. Rahimi-Keshari, A. Scherer, A. Mann, A. T. Rezakhani, A. Lvovsky, and B. C. Sanders, Quantum process tomography with coherent states, New J. Phys. **13**, 013006 (2011).
[18] A. Anis and A. Lvovsky, Maximum-likelihood coherent-state quantum process tomography, New J. Phys. **14**, 105021 (2012).
[19] S. Ahmed, F. Quijandría, and A. F. Kockum, Gradient-descent quantum process tomography by learning Kraus operators, Phys. Rev. Lett. **130**, 150402 (2023).
[20] B. Vlastakis, G. Kirchmair, Z. Leghtas, S. E. Nigg, L. Frunzio, S. M. Girvin, M. Mirrahimi, M. H. Devoret, and R. J. Schoelkopf, Deterministically encoding quantum information using 100-photon Schrodinger cat states, Science **342**, 607 (2013).
[21] P. Campagne-Ibarcq, A. Eickbusch, S. Touzard, E. Zalys-Geller, N. E. Frattini, V. V. Sivak, P. Reinhold, S. Puri, S. Shankar, R. J. Schoelkopf, L. Frunzio, M. Mirrahimi, and M. H. Devoret, Quantum error correction of a qubit encoded in grid states of an oscillator, Nature (London) **584**, 368 (2020).
[22] A. Eickbusch, V. Sivak, A. Z. Ding, S. S. Elder, S. R. Jha, J. Venkatraman, B. Royer, S. M. Girvin, R. J. Schoelkopf, and M. H. Devoret, Fast universal control of an oscillator with weak dispersive coupling to a qubit, Nat. Phys. **18**, 1464 (2022).
[23] M. Kudra, M. Kervinen, I. Strandberg, S. Ahmed, M. Scigliuzzo, A. Osman, D. P. Lozano, M. O. Tholén, R. Borgani, D. B. Haviland *et al.*, Robust preparation of Wigner-negative states with optimized SNAP-displacement sequences, PRX Quantum **3**, 030301 (2022).
[24] M. Reagor, W. Pfaff, C. Axline, R. W. Heeres, N. Ofek, K. Sliwa, E. Holland, C. Wang, J. Blumoff, K. Chou, M. J. Hatridge, L. Frunzio, M. H. Devoret, L. Jiang, and R. J. Schoelkopf, Quantum memory with millisecond coherence in circuit QED, Phys. Rev. B **94**, 014506 (2016).
[25] M. Kudra, J. Biznárová, A. Fadavi Roudsari, J. J. Burnett, D. Niepce, S. Gasparinetti, B. Wickman, and P. Delsing, High quality three-dimensional aluminum microwave cavities, Appl. Phys. Lett. **117**, 070601 (2020).
[26] J. Koch, T. M. Yu, J. Gambetta, A. A. Houck, D. I. Schuster, J. Majer, A. Blais, M. H. Devoret, S. M. Girvin, and R. J. Schoelkopf, Charge-insensitive qubit design derived from the Cooper pair box, Phys. Rev. A **76**, 042319 (2007).
[27] See Supplemental Material at http://link.aps.org/supplemental/10.1103/PhysRevA.110.L020401 for additional information about the experimental and theoretical methods, which includes Refs. [43,46,47].
[28] L. Hu, Y. Ma, W. Cai, X. Mu, Y. Xu, W. Wang, Y. Wu, H. Wang, Y. P. Song, C.-L. Zou, S. M. Girvin, L.-M. Duan, and L. Sun, Quantum error correction and universal gate set operation on a binomial bosonic logical qubit, Nat. Phys. **15**, 503 (2019).
[29] R. W. Heeres, B. Vlastakis, E. Holland, S. Krastanov, V. V. Albert, L. Frunzio, L. Jiang, and R. J. Schoelkopf, Cavity state manipulation using photon-number selective phase gates, Phys. Rev. Lett. **115**, 137002 (2015).
[30] S. Krastanov, V. V. Albert, C. Shen, C.-L. Zou, R. W. Heeres, B. Vlastakis, R. J. Schoelkopf, and L. Jiang, Universal control of an oscillator with dispersive coupling to a qubit, Phys. Rev. A **92**, 040303(R) (2015).
[31] T. Fösel, S. Krastanov, F. Marquardt, and L. Jiang, Efficient cavity control with SNAP gates, arXiv:2004.14256.
[32] S. M. Girvin, Introduction to quantum error correction and fault tolerance, SciPost Phys. Lect. Notes **70** (2023).
[33] J. Helsen, F. Battistel, and B. M. Terhal, Spectral quantum tomography, npj Quantum Inf. **5**, 74 (2019).
[34] M. A. Nielsen, A simple formula for the average gate fidelity of a quantum dynamical operation, Phys. Lett. A **303**, 249 (2002).
[35] A. S. Fletcher, P. W. Shor, and M. Z. Win, Optimum quantum error recovery using semidefinite programming, Phys. Rev. A **75**, 012338 (2007).
[36] J. M. Chow, J. M. Gambetta, A. D. Corcoles, S. T. Merkel, J. A. Smolin, C. Rigetti, S. Poletto, G. A. Keefe, M. B. Rothwell, J. R. Rozen *et al.*, Universal quantum gate set approaching fault-tolerant thresholds with superconducting qubits, Phys. Rev. Lett. **109**, 060501 (2012).
[37] C. J. Wood and J. M. Gambetta, Quantification and characterization of leakage errors, Phys. Rev. A **97**, 032306 (2018).
[38] J. R. Johansson, P. D. Nation, and F. Nori, QuTiP: An open-source Python framework for the dynamics of open quantum systems, Comput. Phys. Commun. **183**, 1760 (2012).
[39] J. R. Johansson, P. D. Nation, and F. Nori, QuTiP 2: A Python framework for the dynamics of open quantum systems, Comput. Phys. Commun. **184**, 1234 (2013).
[40] C. R. Harris, K. J. Millman, S. J. van der Walt, R. Gommers, P. Virtanen, D. Cournapeau, E. Wieser, J. Taylor, S. Berg, N. J. Smith, R. Kern, M. Picus, S. Hoyer, M. H. van Kerkwijk, M. Brett, A. Haldane, J. F. del Río, M. Wiebe, P. Peterson, P. Gérard-Marchant, K. Sheppard, T. Reddy, W. Weckesser, H. Abbasi, C. Gohlke, and T. E. Oliphant, Array programming with NumPy, Nature (London) **585**, 357 (2020).
[41] J. D. Hunter, Matplotlib: A 2D graphics environment, Comput. Sci. Eng. **9**, 90 (2007).
[42] J. Bradbury, R. Frostig, P. Hawkins, M. J. Johnson, C. Leary, D. Maclaurin, G. Necula, A. Paszke, J. VanderPlas, S. Wanderman-Milne, and Q. Zhang, JAX: Composable transformations of Python+NumPy programs, https://github.com/google/jax (2018).
[43] R. A. Bertlmann and P. Krammer, Bloch vectors for qudits, J. Phys. A **41**, 235303 (2008).
[44] D. Willsch, Supercomputer simulations of transmon quantum computers, Ph.D. thesis, RWTH Aachen University, 2020.
[45] F. Jin, D. Willsch, M. Willsch, H. Lagemann, K. Michielsen, and H. de Raedt, Random state technology, J. Phys. Soc. Jpn. **90**, 012001 (2021).
[46] P. Reinhold, Controlling error-correctable bosonic qubits, Ph.D. thesis, Yale University, 2019.
[47] C. J. Wood, J. D. Biamonte, and D. G. Cory, Tensor networks and graphical calculus for open quantum systems, Quant. Inf. Comp. **15**, 0579 (2015).